Cite this paper as: Organometallics, **2018**, *37*, 327-336, DOI: acs.organomet.7b00739

Zn(II) byproduct enhances the Cu-catalyzed cross-coupling of bromozinc-difluorophosphonate with iodobenzoates: A DFT study

Jesús Jover

Departament de Química Inorgànica i Orgànica, Secció de Química Inorgànica and Institut de Química Teòrica i Computacional (IQTC-UB), Universitat de Barcelona, Martí i Franquès 1-11, 08028 Barcelona, Spain.
Institute of Chemical Research of Catalonia (ICIQ), The Barcelona Institute of Science and Technology, Avgda. Països Catalans, 16, 43007 Tarragona, Spain.

ABSTRACT

The copper-catalyzed cross-coupling of bromozinc-difluorophosphonate with iodobenzoates has been studied with DFT methodology in order to understand the experimentally observed reactivity. The directing carboxylate group promotes the reaction for methyl 2-iodobenzoate and, unexpectedly, also for methyl 4-iodobenzoate, although to a lesser extent. DFT calculations show that the Zn(II) byproduct, formed in the initial stages of the reaction, remains attached to the catalyst and serves as anchoring point for the benzoate moiety allowing, in turn, the reaction for both *ortho*- and *para*-substituted iodobenzoates. The computationally derived reaction mechanism has also been applied to study whether other substrates may engage in a similar cross-coupling process with bromozinc-difluorophosphonate. The calculations carried out on substrates bearing nitrogen-directing groups, such as triazene and pyridine, indicate that their reactions should be possible and the latter should produce a much faster reaction than iodobenzoates.

INTRODUCTION

Over the last years organofluorine chemistry has emerged and attracted the attention of the chemistry community. Indeed, fluorinated compounds have become a major research topic in pharmaceutical and agrochemical industries as the presence of fluorine often improves the metabolic stability, bioavailability and lipophilicity of organic moieties.[1] Most efforts in this research area have been devoted to the introduction of fluorine (-F) or the trifluoromethyl ($-CF_3$) group in organic compounds[2] while the synthesis of difluoromethylated molecules has been less explored.[3] Even so, the difluoromethylene group ($-CF_2$) has become one of the most interesting targets in organofluorine chemistry because it can act, for example, as a bioisostere of a carbonyl group or an oxygen atom. One of the most promising candidates among all the existing difluoromethylenic groups is the $-CF_2P(O)(OR)_2$ residue, which can be considered as a stable *in vivo* mimetic of the phosphate group such as those present in natural molecules and enzimes.[4]

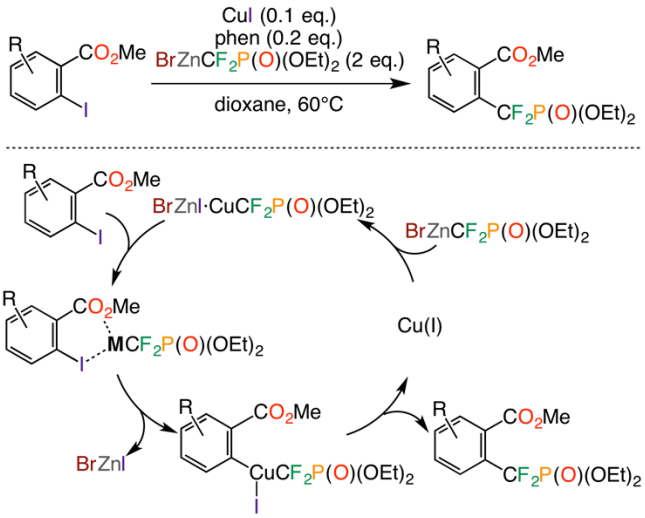

Scheme 1. Copper-catalyzed cross-coupling of iodobenzoates with bromozinc-difluorophosphonate (top) and mechanism of the reaction as proposed by Zhang *et al*. (bottom).

One of the main developments in this field was reported by Zhang and coworkers in 2012 (Scheme 1, top).[5] Their reaction was the first example of copper-catalyzed cross-coupling of iodobenzoate with a bromozinc-difluorophosphonate counterpart and allowed the preparation of aryldifluorophosphonates with excellent functional group compatibillity and high efficiencies. The experiments indicated that the reaction did not proceed through a radical mechanism and therefore a more classical oxidative addition/reductive elimination cross-coupling mechanism was proposed (Scheme 1, bottom). The reaction mechanism states that the incoming substrate interacts with an organocopper zinc species (**M** in Scheme 1) prior to the oxidative addition of the C–I bond onto the copper atom, which is facilitated by the benzoate moiety placed in *ortho* to the iodide and enables the overall catalytic cycle. Interestingly, the methyl 4-iodobenzoate substrate, where the iodide and the directing carboxylate group are placed in *para* positions, is also able to engage in the cross-coupling reaction, although with poorer results (< 20% yield). This indicates that the reaction is still able to proceed despite having a strong *ortho*-directing group, which should be expected to prevent any type of reactivity. In any case, the presence of the directing group is essential for the catalytic reaction to proceeed; in this line, previous studies of Shibuya and coworkers[6] demonstrated that carrying out a similar cross-coupling process without a directing group in the substrate required a stoichimetric amount of copper and produced a radical single electron transfer (SET) reaction mechanism.

In this report the catalytic cycle proposed by Zhang and coworkers, including three different plausible pathways, will be computationally studied using methyl 2-iodobenzoate as substrate. Once the reaction mechanism has been established it will be used to understand the unexpected reactivity shown by methyl 4-iodobenzoate. Finally, the reaction mechanism will be evaluated for two different substrates bearing the N-directing triazene and pyridine groups, *i.e.* using 1-((2-

iodophenyl)diazenyl)piperidine and phenyl 2-(2-iodophenyl)pyridine, to check whether they would make good partners for the studied reaction.

EXPERIMENTAL SECTION

Computational Details

All the structures have been fully optimized using 1,4-dioxane as solvent (PCM, see below) using the Gaussian09[7] package with B3LYP functional.[8] In the optimization process the standard 6-31G* basis set[9] is used for all H, C, N, O, F, and P atoms while the Stuttgart triple zeta basis set (SDD),[10] along with the associated ECP to describe the core electrons, has been employed for Cu, Zn, Br and I. Tight convergence criteria as well as ultrafine integration grids have been used in order to ensure satisfactory convergence. In all cases the solvation energies are computed in 1,4-dioxane with the (IEF-PCM)[11] continuum dielectric solvation model using the SMD[12] radii and non-electrostatic terms. The dispersion correction terms have been included in all the calculations by using the D3 method of Grimme.[13] These computational settings are named BS1. Frequency calculations are carried out after each optimization to ensure the nature of stationary points and transition states, which have zero and one imaginary frequencies, respectively. Additional single point calculations, including solvation and dispersion corrections, on the optimized geometries are employed to obtain improved Gibbs energy values with larger basis sets (BS2). The aug-cc-pVTZ-PP[14] basis set including polarization and the associated electron core potential has been employed for Cu, Zn, Br and I while the 6-311+G** basis set[9c,15] is used for all the other atoms. The computed Gibbs energies have been corrected to use a standard state corresponding to species in solution with a standard concentration of 1 M. Unless otherwise stated all the Gibbs energy values in the text correspond to those computed with the larger basis sets BS2 including PCM-SMD solvation and the D3 dispersion terms at 60°C. The detailed procedure to obtain these Gibbs energy values is described in the ESI. These computational settings have been previously employed in other copper-catalyzed reactions and have been shown to produce accurate results.[15] Nevertheless, some of the calculations reported here have been repeated with the PBE0[16] and B97D[17] functionals, and observed to produce very similar results. Special care has been taken when modeling the organometallic species involved in the computed catalytic cycles; in this case, one of the potential important issues is the change on the coordination number of the metal centers along the computed pathways, typically by the binding of substrate or explicit solvent molecules. The calculations indicate that tricoordinated copper(I) complexes do not tend to become tetracoordinated by binding additional solvent molecules. On the other hand, zinc(II) always prefers adopting a tetrahedral geometry and, whenever necessary, explicit 1,4-dioxane solvent molecules have been added/removed to maintain the tetracoordination along the reaction. This is reflected in all the schemes included in this report; the coordination number around the copper atoms always corresponds to the number of bound ligands in the schemes. In contrast, zinc remains tetrahedral and hence the coordination number is always equal to four; this means that whenever a di- or tricoordinated Zn species appear in a scheme, two or one solvent

molecules have been added, respectively, to complete the tetrahedral coordination sphere. Of course, the solvent binding/release processes onto zinc are considered to take place by diffusion and therefore they are assumed to be barrierless.

RESULTS AND DISCUSSION

The catalytic cycle originally proposed by Zhang and coworkers can be interpreted in different ways depending on the nature of the key species formed prior to the oxidative addition step *i.e.* **M** in Scheme 1. The substrate coordination onto the organocopper zinc species, binding either to copper or zinc, provides different reaction pathways that should be studied. For this reason, three different pathways, all of them complying with the experimental observations, have been computed. Of course, the proposed catalytic cycles are just that, proposals that come to terms with the experiments and allow the interpretation of the underlying chemical process. Obviously there is always room for potential alternative mechanisms that have not been computed and may be also possible. Nevertheless, the calculations presented in this report, incomplete as they may be, allow explaining the observed reactivity, provide sensible energy barriers and remain simple enough to be easily interpreted.

The first attempt to describe the catalytic cycle of the reaction proposed by Zhang and coworkers, including the relative Gibbs energies in 1,4-dioxane at 65°C of all the species involved (in kcal mol^{-1}), is shown in Scheme 2 and named Pathway 1 throughout this report. The reaction should start by the coordination of the preformed [$ZnBr(CF_2P(O)(OEt)_2)$] species to the initial copper(I) catalyst (**I1**) to produce intermediate (**I2**); this process is exergonic and the latter intermediate is found almost 7 kcal mol^{-1} below the separated reactants. Since the copper atom in **I1** is coordinatively unsaturated this process is likely to be driven by diffusion processes instead of governed by an energy barrier. In **I2** the phosphonate oxide group is bound to the copper and, at the same time, the zinc approaches the iodide; the Cu–O and Zn–I distances are 2.29 and 2.75 Å, respectively; as a consequence, the initial Cu–I distance elongates from 2.50 (**I1**) to 2.57 Å (**I2**). After that the fluorinated phosphonate group ($CF_2P(O)(OEt)_2$) has to be transferred from the zinc to the copper center through the corresponding transmetalation transition state (**TMTS**, Figure 1 left), which would lead to the formation of intermediate **I3**. In this transition state the distance between both copper and zinc atoms becomes as short as 2.37 Å, well below the sum of both van der Waals radii for those metals and possibly indicating a certain character of metal-metal bond character. As may be observed the position of the P=O group varies between **I2** (on Cu) and **TMTS** (on Zn), showing that this substituent switches between both metals. It may then be argued that these two species are not directly connected and the species prior to transmetalation may not be **I2**; however, all the other computed isomers of **I2** are found at higher energies *e.g.* the double-halide bridging species can be found at -3.0 kcal mol^{-1} while the complex with only iodide bridging both metals –and possibly the species leading to **TMTS**– has also a relative Gibbs energy value of -3.0 kcal mol^{-1}.

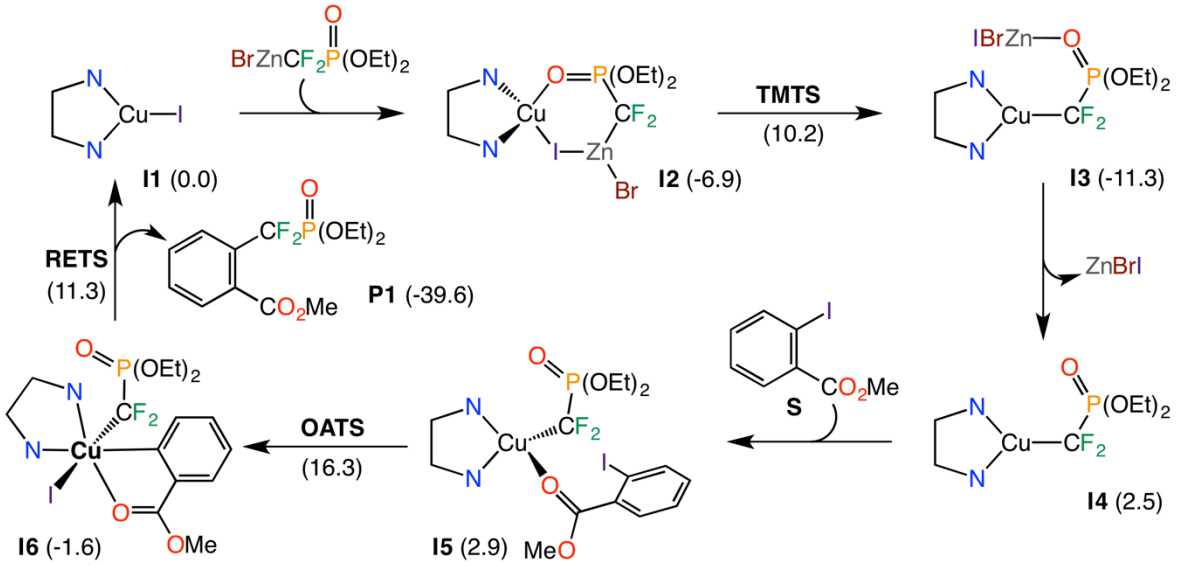

Scheme 2. Computed reaction Pathway 1, including relative Gibbs energies in kcal mol^{-1}, for the cross-coupling of bromozinc-difluorophosphonate with methyl 2-iodobenzoate (NN ligand = phenanthroline, the copper oxidation state is given by color: Cu = Cu(I), **Cu** = Cu(III)).

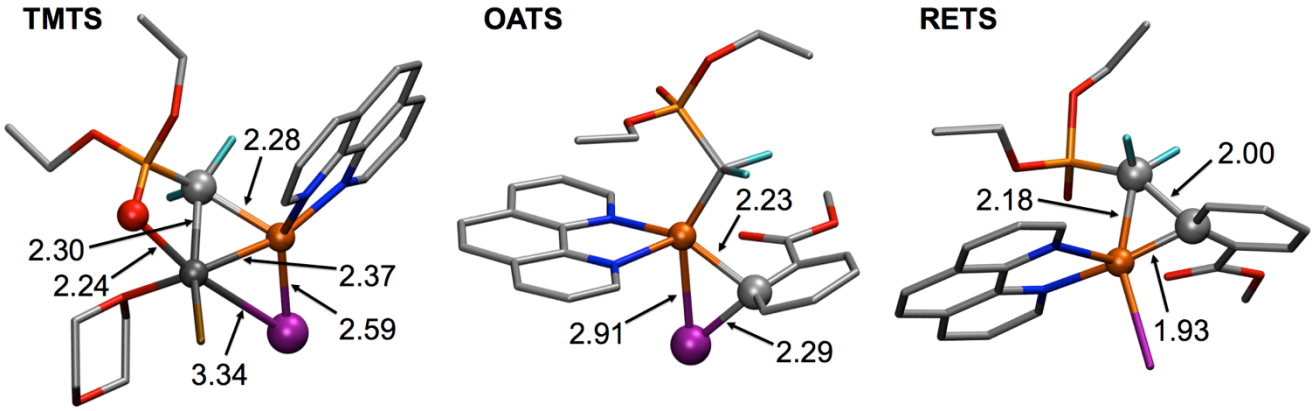

Figure 1. Transition states along Pathway 1 for substrate **S**: left = transmetalation (**TMTS**), middle = oxidative addition (**OATS**) and right = reductive elimination (**RETS**). Color code: Cu = copper, Zn = black, C = gray, N = blue, O = red, F = cyan, P =orange, Br = brown, I = purple, for clarity H-atoms have been omitted. Atoms represented as balls are those actively participating in the transition state motions. All distances are given in Å.

This latter species should be easily obtained by a rotation of the Zn–C–P–O torsion angle in **I2**, which would move the P=O group away from the copper atom. Since **I2** has the lowest relative Gibbs energy it is the most likely intermediate to be formed prior to transmetalation. Once **I3** is obtained the reaction should proceed by the release of [ZnBrI(1,4-dioxane)$_2$] and the formation of the copper(I) complex **I4**. This step has a quite large energy requirement –more than 13 kcal mol^{-1} are required– and thus the liberation of the Zn byproduct seems to be quite unlikely. A plausible

solution for this issue is presented in the next paragraphs but, for the moment, the explanation will remain in this catalytic cycle. After the release of [ZnBrI(1,4-dioxane)$_2$] **I4** should bind a methyl 2-iodobenzoate molecule (**S**) to deliver intermediate **I5**. In this copper(I) complex the carboxylate group directly interacts with the metal center and the Cu–O distance is 2.40 Å. As may be observed the interaction between these two fragments does not seem to be extremely strong and the coordination process is practically thermoneutral, with **I4** and **I5** having practically equal relative Gibbs energies. The next step of the reaction should be the oxidative addition of the C–I bond of the incoming substrate onto the metal to form the copper(III) complex **I6**. The formation of this kind of complexes, often invoked in non-radical copper-catalyzed reactions, has become widely accepted in recent times.[18] And this is mainly because of the new experimental evidences obtained from advanced spectroscopic techniques and the study of catalyst models, which allow the identification and characterization of these elusive species.[19] The oxidative addition process is governed by the corresponding transition state (**OATS**, Figure 1 middle) in which the two carbon substituents are placed *cis* to each other. Of course, other oxidative addition transition states exist but those that were computed displayed higher energy requirements or lead to unproductive pathways, *e.g.* the transition state placing the iodide between the phenyl and the $CF_2P(O)(OEt)_2$ groups has a relative Gibbs energy value of 19.5 kcal mol^{-1}, while **OATS**, although endergonic, is found at a relative Gibbs energy of 16.3 kcal mol^{-1}. In **OATS**, the C_{ipso}–I, Cu–C_{ipso} and Cu–I distances are 2.29, 2.23 and 2.91 Å, respectively, remaining in their typical range for this kind of structures. Nevertheless, it is worth noting that the distance between the copper atom and the carboxylate largely increases in this transition state (3.07 Å), indicating that the directing group effect seems to be quite limited. Intermediate **I6** exhibits a distorted octahedral geometry around the copper(III) center, with two long axial distances. The two axial positions are occupied by the carboxylate group of the benzoate (at 2.58 Å) and one of the nitrogen atoms of phenanthroline (at 2.48 Å). The particular arrangement of **OATS** dictates that both carbon substituents: the benzoate ring and $CF_2P(O)(OEt)_2$ lie *cis* to each other in complex **I6**. This complex has a relatively low value of Gibbs energy (-1.6 kcal mol^{-1}) and is the most stable among all the possible copper(III) conformers that can be computed, probably because the *trans*-influence of the substituents present is well balanced: $C_{benzoate}$ *vs.* N_{phen}, $C_{CF_2P(O)(OEt)_2}$ *vs.* I, and N_{axial} *vs.* O_{axial}. Getting the product from **I6** should be quite straightforward by a C–C reductive elimination; the transition state governing this transformation (**RETS**, Figure 1 right) is found just 12.9 kcal mol^{-1} higher than the previous intermediate, demonstrating that this barrier should be very easily overcome under the experimental conditions. In **RETS** the distance between both carbon groups becomes quite short (2.00 Å) while the Cu–$C_{benzoate}$ distance remains practically unchanged (1.93 Å compared to 1.91 Å in **I6**). It is also worth noting that in this case, and in contrast to **OATS**, the distance between the copper atom and the carboxylate group is relatively short (2.60 Å). After the reductive elimination the product (**P1**) is released into the reaction mixture and the starting catalyst species (**I1**) is recovered to engage

in successive cycles. The overall thermodynamics indicate that the studied reaction is exergonic by 39.6 kcal mol^{-1}. The computed relative Gibbs energies allow the calculation of the apparent activation energy for the studied reaction, which is directly related to its turnover frequency. This can be easily done by means of the energetic span model developed by Kozuch and Shaik.[20] This model states that the activation barrier corresponds to the energy difference between the highest and the lowest species when the latter appears first in the catalytic cycle, as in this case. Therefore, the activation barrier for a reaction following Pathway 1 has a value of 27.6 kcal mol^{-1}, obtained as the energy difference between **I3** and **OATS**. This value seems to be relatively high for a reaction that is near to completion after 24 hours at 60°C, and this is probably due to the large energy investment needed to release [ZnBrI(1,4-dioxane)$_2$] from intermediate **I3**. Since this species cannot be easily released, an alternative to lower the activation barrier could be keeping this fragment attached to the catalyst throughout the catalytic cycle. This new catalytic cycle, named Pathway 2 (Scheme 3, left), is equivalent to the one shown in Scheme 1; the only difference being the elimination of the stage where the [ZnBrI(1,4-dioxane)$_2$] fragment is expelled (**I3 → I4**). However, keeping the zinc byproduct bound to the P=O group along the reaction has an unexpected and crucial implication; for while Zn remains in the catalyst it can also coordinate to the carboxylate group of the substrate to produce a viable catalytic cycle (Pathway 3, Scheme 3, right). Thus, these two new plausible catalytic cycles have been computed and analyzed. Pathway 2 starts from intermediate **I3**, which is a common species to all the studied pathways, and should proceed by the coordination of one molecule of methyl 2-iodobenzoate (**S**). This process, which is slightly endergonic, produces complex **I7,** where the substrate binds to the copper through the carboxylate group (the Cu–O distance is 2.30 Å, a bit shorter to that in intermediate **I5** (2.40 Å)). After that the oxidative addition of the C–I bond onto the copper center should take place and complex **I8** would be formed. This step is controlled by the corresponding transition state (**OATS2**) that requires further 19.8 kcal mol^{-1}; this energy requirement is larger than that of the equivalent oxidative addition in Pathway 1 (**OATS**, 13.4 kcal mol^{-1}). The resulting copper(III) complex (**I8**) is quite low in energy and has the same spatial arrangement than the analogous intermediate in Pathway 1 (**I6**). The C–C reductive elimination produces the final product containing the [ZnBrI(1,4-dioxane)$_2$] -bound moiety (**P2**) and allows the recovery of the initial copper (I) catalyst (**I1**). The transition state governing this transformation (**RETS2**) has an energy demand of 13.3 kcal mol^{-1}, slightly larger than that of Pathway 1 (12.9 kcal mol^{-1}). Step by step, it seems that all the processes require a larger amount of energy in Pathway 2 when compared to Pathway 1; nevertheless, the apparent activation barrier in this catalytic cycle, computed as the Gibbs energy difference between **I3** and **OATS2**, is much lower (27.6 *vs.* 20.4 kcal mol^{-1} for Pathways 1 and 2, respectively) since the energy penalty of liberating [ZnBrI(1,4-dioxane)$_2$] into the reaction mixture is avoided.

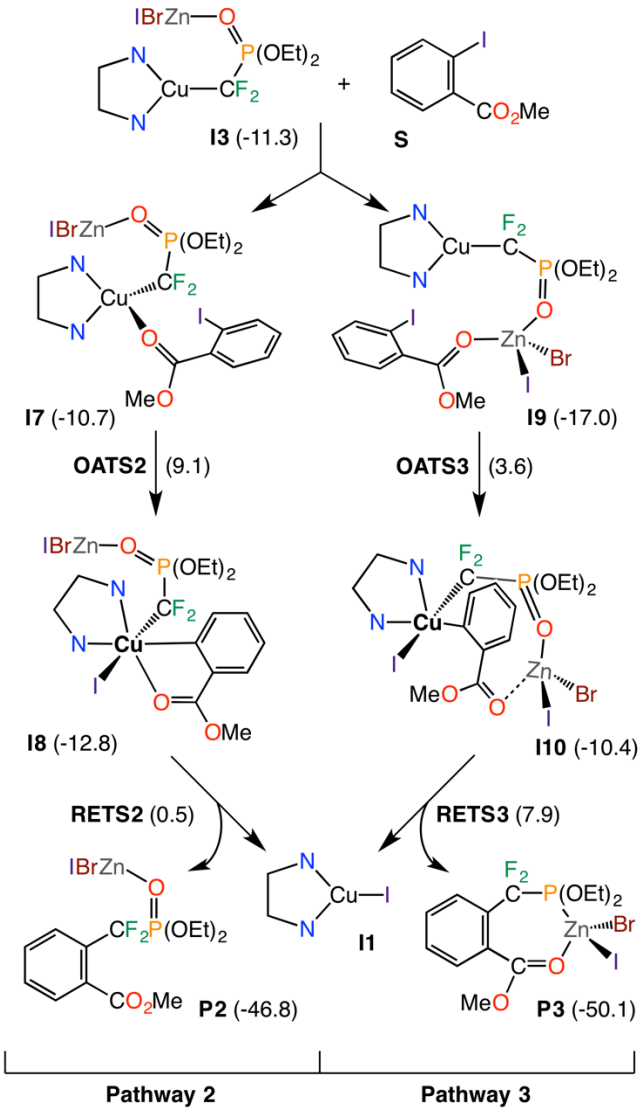

Scheme 3. Alternative reaction pathways, including relative Gibbs energies in kcal mol^{-1}, for the cross-coupling of bromozinc-difluorophosphonate with methyl 2-iodobenzoate (NN ligand = phenanthroline, the copper oxidation state is given by color: Cu = Cu(I), **Cu** = Cu(III)).

The alternative reaction mechanism named as Pathway 3, where the methyl 2-iodobenzoate substrate (**S**) binds onto zinc instead of copper, is shown in Scheme 3 (right). As may be observed the interaction between the carboxylate group and Zn to form intermediate **I9** is clearly favored when compared to its copper analog (**I7**): -17.0 vs. -10.7 kcal mol^{-1}, respectively. The short Zn–O distance in **I9** (2.15 Å) also indicates the strength of the interaction between both reactants. Alternatively, the substrate was made to interact with the zinc fragment through the iodide group; the resulting structure shows a quite long Zn–$I_{substrate}$ distance (3.21 Å) and a relative Gibbs energy around 5 kcal mol^{-1} higher than that of **I9**, indicating that this arrangement is not plausible to occur during the reaction. The flexibility of the dangling phosphonate group should allow the substrate to orient towards the copper center so the oxidative addition can take place.

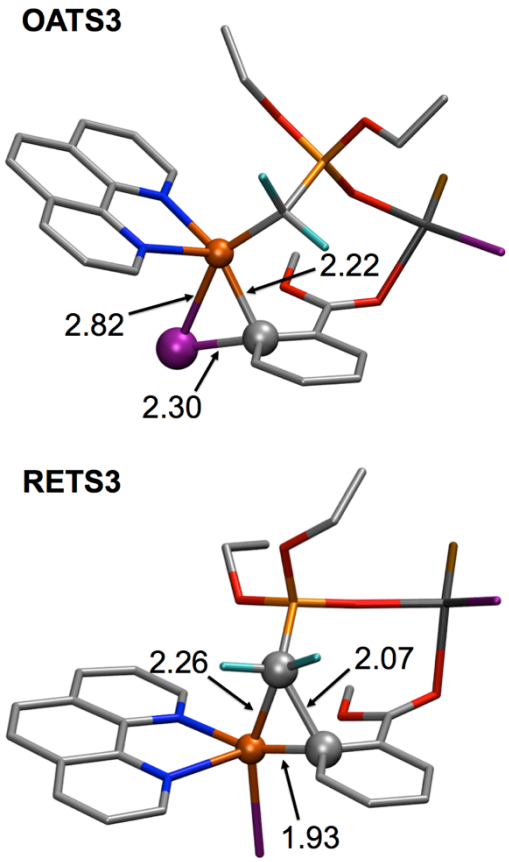

Figure 2. Transition states along Pathway 3 for substrate **S**: top = oxidative addition (**OATS3**) and bottom = reductive elimination (**RETS3**). Color code: Cu = copper, Zn = black, C = gray, N = blue, O = red, F = cyan, P =orange, Br = brown, I = purple, for clarity H-atoms have been omitted. Atoms represented as balls are those actively participating in the transition state motions. All distances are given in Å.

The transition state mediating the C–I bond cleavage onto the Cu atom (**OATS3**, Figure 2 top) is 20.6 kcal mol^{-1} above **I9**. This oxidative addition process is more energy demanding than those in Pathways 1 and 2: 13.4 and 19.8 kcal mol^{-1} for **OATS1** and **OATS2**, respectively, but should be still easily overcome at 60°C. As may be observed, the C_{ipso}–I, Cu–C_{ipso} and Cu–I distances in **OATS3** (2.30, 2.29 and 2.82 Å, respectively) are very similar to those obtained in the oxidative addition where the substrate is directly bound to the copper center (**OATS**) and thus the higher energy requirement of **OATS3** is probably due to the different conformation of the phosphonate-[ZnBrI] group. After the oxidative addition step the copper(III) complex **I10** should be formed; in contrast to Pathways 1 and 2, this complex is higher in energy than the previous intermediate but still remains at an acceptable level. Intermediate **I10** displays a square pyramidal geometry around the copper atom, with one of the phenanthroline nitrogen donor atoms placed in the axial position and the difluorophosphonate and the benzoate positioned *cis* to each other. The C–C reductive elimination (**RETS3**, Figure 2 bottom) from **I10** seems to be quite straightforward

and requires 18.3 kcal mol^{-1}. This energy demand is again larger than those corresponding to **RETS** and **RETS2** (12.9 and 13.3 kcal mol^{-1}, respectively), probably due to the conformational strain introduced by the phosphonate-[ZnBrI] group. The C_{CF_2}–C_{ipso}, Cu–C_{ipso} and Cu–C_{CF_2} distances in **RETS3** (2.07, 1.93 and 2.26 Å, respectively) are also similar to those observed for the copper-bound substrate (**RETS)**. Once the C–C bond has been formed the cyclometalated product (**P3**) should be obtained and the initial catalytic species (**I1**) would be recovered, ready to engage in successive reaction cycles. The apparent activation barrier associated to Pathway 3, calculated as the Gibbs energy difference between **I9** and **RETS3**, is 24.9 kcal mol^{-1}, which corresponds to the actual lowest Gibbs energy barrier of the whole reaction. And this is because the barriers for Pathways 1 and 2 have to be updated and computed against the lowest intermediate throughout, which happens to be **I9**. By doing so those barriers rise to 33.3 and 26.1 kcal mol^{-1} for Pathways 1 and 2, respectively (Scheme 4).

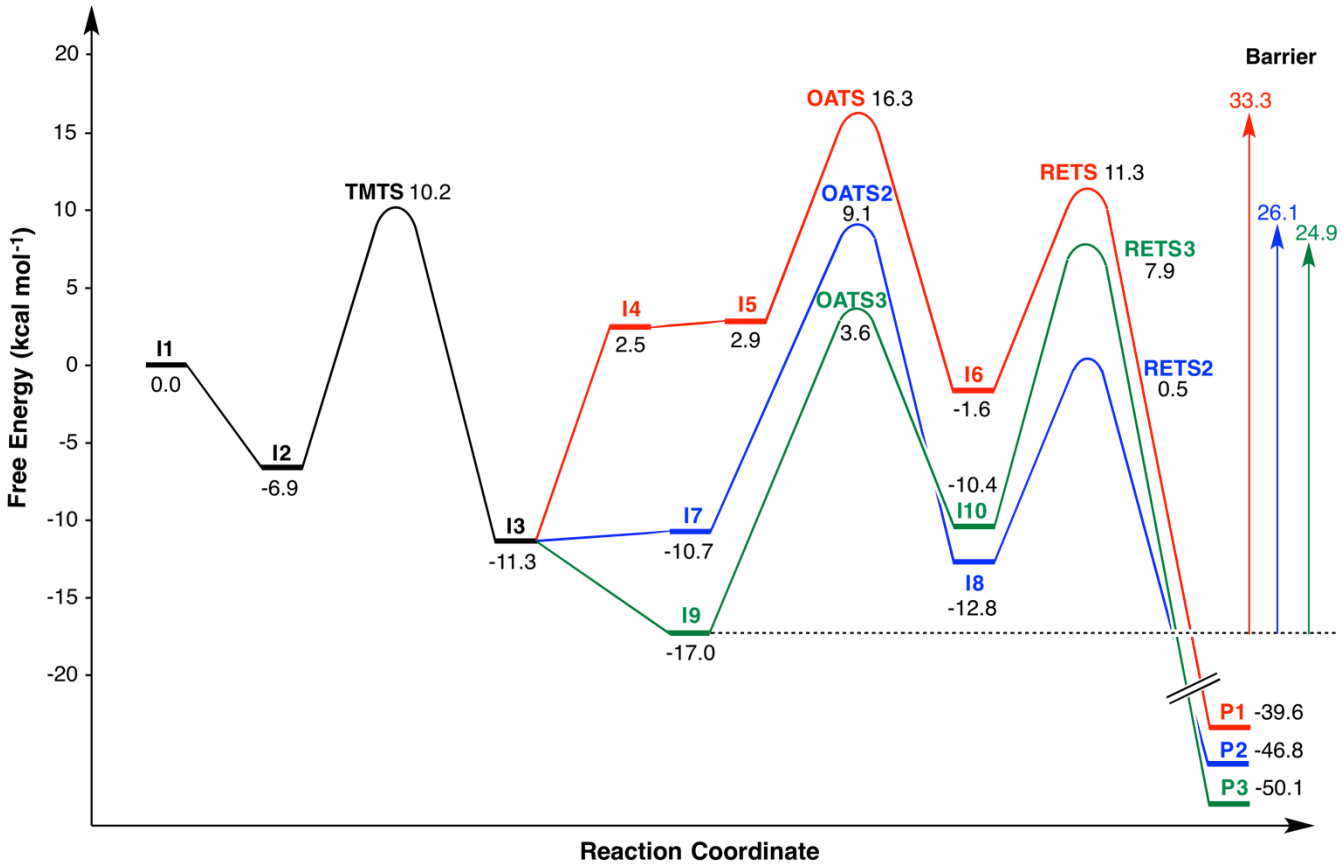

Scheme 4. Gibbs energy profiles (in kcal mol^{-1}) for Pathways 1 (red), 2 (blue) and 3 (green) in the copper-catalyzed cross-coupling of methyl 2-iodobenzoate with bromozinc-difluorophosphonate, and apparent activation barriers for each pathway from the resting state **I9**.

The relative barrier heights for each pathway indicate that the vast majority of the final product should be obtained from Pathway 3 (**P3**), although some **P2** could be also formed. In the same line it seems that Pathway 1 could be safely ruled out. However, and as stated in the original experimental report, after 24 h "the reaction mixture was cooled to room temperature, and diluted with EtOAc, washed with brine, dried over Na_2SO_4, filtered and concentrated",[5] which means that at the end of the reaction **P1** –if some–, **P2** and **P3** should be combined in a single fraction, most probably free of [ZnBrI(1,4-dioxane)$_2$].The computed reaction mechanism for methyl 2-iodobenzoate (**S**), which confirms the existence and effectiveness of Pathway 3, allows understanding why the similar methyl 4-iodobenzoate substrate (**S2**) is able to cross-couple with the copper catalyst regardless of the *ortho*-directing carboxylate group absence. As before, the conformational flexibility of the phosphonate-[ZnBrI] fragment allows the reaction to be directed to the *para*-position of the substrate (Scheme 5).

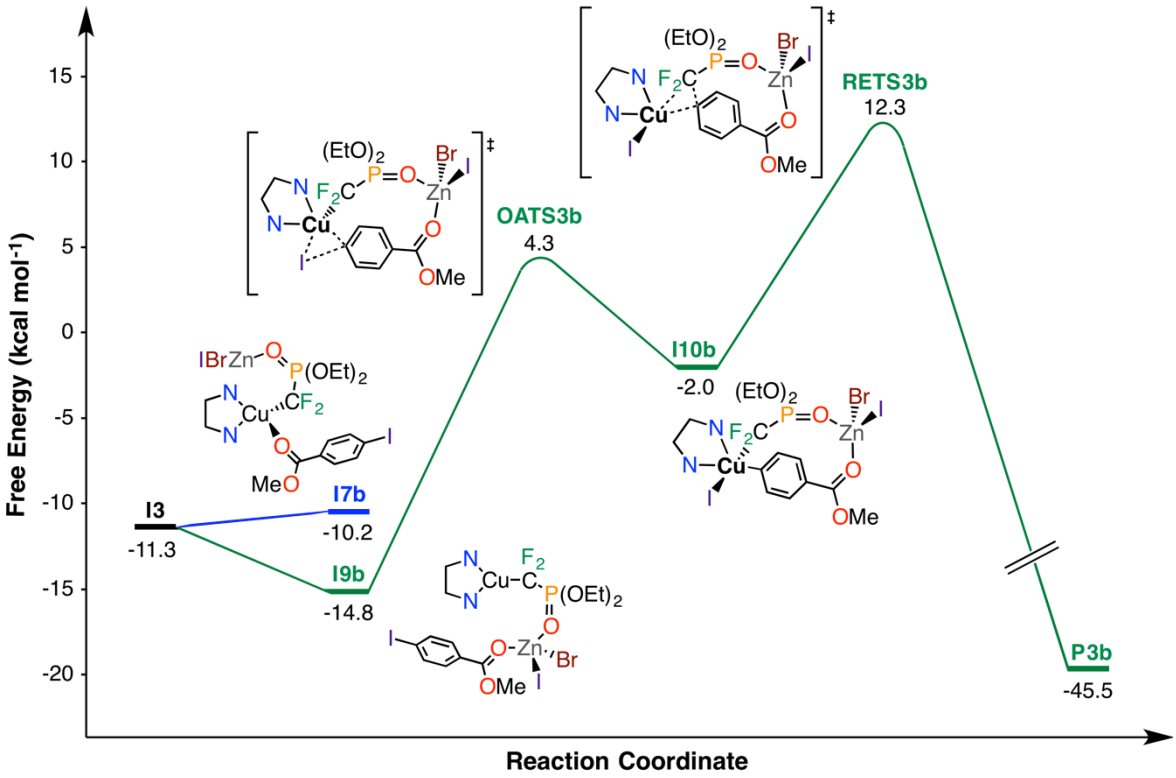

Scheme 5. Gibbs energy profiles (in kcal mol^{-1}) for Pathways 2 (blue) and 3 (green) in the copper-catalyzed cross-coupling of methyl 4-iodobenzoate (**S2**) with bromozinc-difluorophosphonate, starting from **I3** (NN ligand = phenanthroline, the copper oxidation state is given by color: Cu = Cu(I), **Cu** = Cu(III)).

The reaction mechanism for **S2** follows the same sequence as the ones computed above. Since Pathway 1 displays a very high Gibbs energy barrier it has not been computed for this substrate. Pathway 2 should not be operative for **S2** because the coordination of the substrate directly to the copper atom, delivering intermediate **I7b**,

inhibits the reaction by preventing the oxidative addition to happen. In addition, this type of coordination is slightly endergonic which means that it would probably not interfere with Pathway 3, which seems to become the only plausible reaction mechanism to explain the observed experimental reactivity. The coordination of methyl 4-iodobenzoate to intermediate **I3**, through their respective carboxylate and zinc fragments, is thermodynamically favored and the complex **I9b** is found more than 3 kcal mol^{-1} below the separated molecules. The Zn–O distance in this complex is quite short (2.13 Å), just like the one obtained with the original substrate (**S**) in intermediate **I9**. The C–I bond should be then cleaved onto the copper center to produce intermediate **I10b**; this process is controlled by the corresponding oxidative addition transition state (**OATS3b**) that lies 19.1 kcal mol^{-1} above **I9b**, even lower than that for methyl 2-iodobenzoate (**S**). As may be observed the distances in **OATS3b** (Figure 3, top) are quite different to those obtained in **OATS3** (Figure 2, top). In **OATS3b** the C_{ipso}–I distance is longer whereas the Cu–C_{ipso} and Cu–I distances are shorter than those of **OATS3**, indicating that the former has a late transition state character while the latter seems to be more concerted.

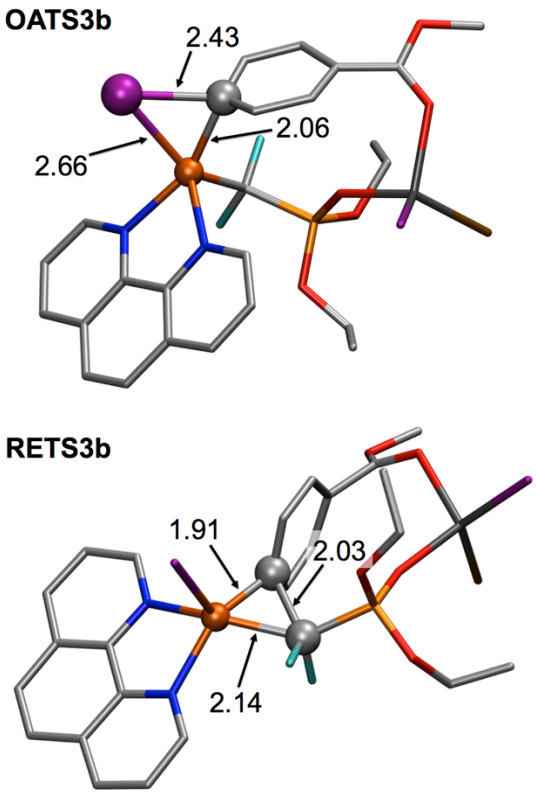

Figure 3. Transition states along Pathway 3 for substrate **S2**: top = oxidative addition (**OATS3b**) and bottom = reductive elimination (**RETS3b**). Color code: Cu = copper, Zn = black, C = gray, N = blue, O = red, F = cyan, P =orange, Br = brown, I = purple, for clarity H-atoms have been omitted. Atoms represented as balls are those actively participating in the transition state motions. All distances are given in Å.

As may be observed, and in contrast to the calculations shown above, the stabilization of the copper(III) intermediate **I10b** is not large, probably because of the strain introduced by the longer cyclometalated fragment. This complex remains almost 13 kcal mol^{-1} higher than **I9b**, which means that the oxidative addition stage should be easily reversible. Intermediate **I10b** shows again a square pyramidal structure around the copper, with one of the phenanthroline nitrogens occupying the axial position while the difluorophosphonate and the benzoate substituents are placed in *cis* at the equatorial plane. The reaction should proceed then by reductively eliminating the CF_2 and the benzoate substituents and forming a new C–C bond; in this way, the final product **P3b** would be obtained and the initial catalyst species (**I**) should be recovered. It has to be noted that **P3b** is not a cyclometalated product, the optimization of this kind of compound always entails the cleavage of the P=O···Zn bond, producing a similar structure to that of **P2**. This final stage is governed by the corresponding reductive elimination transition state (**RETS3b**, Figure 3, bottom), which can be found quite high in energy (overall +11.7 kcal mol^{-1}) along the reaction coordinate. This transition state, unlike **OATS3b**, is similar to its analogous structure for methyl 2-iodobenzoate (**RETS3**), although in this case the Cu–C_{CF_2} distance is a bit shorter. The energy requirement of this reductive elimination process, 14.3 kcal mol^{-1}, is lower than that observed in Pathway 3 for substrate **S** (18.3 kcal mol^{-1}) but this is probably due to the low stabilization of the **I10b** intermediate. The apparent activation barrier associated to Pathway 3 for methyl 4-iodobenzoate (**S2**), obtained as the Gibbs energy difference between **I9b** and **RETS3b**, is 27.1 kcal mol^{-1}. This value is more than 2 kcal mol^{-1} higher than that found for methyl 2-iodobenzoate (**S**), indicating that the cross-coupling reaction of the latter should be much faster, in agreement with what is observed experimentally.

Once a plausible reaction mechanism for the cross-coupling of iodobenzoates with bromozinc-difluorophosphonate has been found it should be easily extended to other similar systems, for example to substrates bearing a nitrogen-directing group instead of a carboxylate. Two different N-donor substrates have been studied, the first one is 1-((2-iodophenyl)diazenyl)piperidine[3c] that has been employed in a very similar reaction, and the potential new substrate phenyl 2-(2-iodophenyl)pyridine, which has not been tested experimentally. These substrates account for triazene and pyridyl N-directing groups, respectively. The reaction mechanism for both these substrates has been computed including only Pathways 2 and 3. 1-((2-iodophenyl)diazenyl)piperidine was reported to participate in as very similar reaction to the one studied here;[3c] in that case the coupling partner was also [$ZnBrCF_2P(O)(OEt)_2$] and the initial catalyst was [Cu(CN)(3,4,7,8-tetramethyl-1,10-phenanthroline)]. The reaction conditions and the solvent were also very similar to the ones and the final results were quite close for both substrates. In conclusion, methyl 2-iodobenzoate and 1-((2-iodophenyl)diazenyl)piperidine should behave in a very similar way in the cross-copupling reaction with the bromozinc difluorophosphonate. The Gibbs energy profiles computed for the copper-catalyzed cross-coupling of 1-((2-iodophenyl)diazenyl)piperidine (**S3**) with bromozinc-difluorophosphonate are shown

in Scheme 6. Since the coordination ability of the triazene directing group is expected to be stronger than that of the carboxylic group this replacement should enhance the interaction between the catalytic species and the substrate, either binding through copper or zinc. In practice, the coordination through zinc is much more favorable (*i.e.* the relative Gibbs energy of **I9c** is almost 10 kcal mol^{-1} lower than that of **I7c**) and the reaction should, in principle, follow Pathway 3; nevertheless, Pathway 2 has been fully computed for completeness.

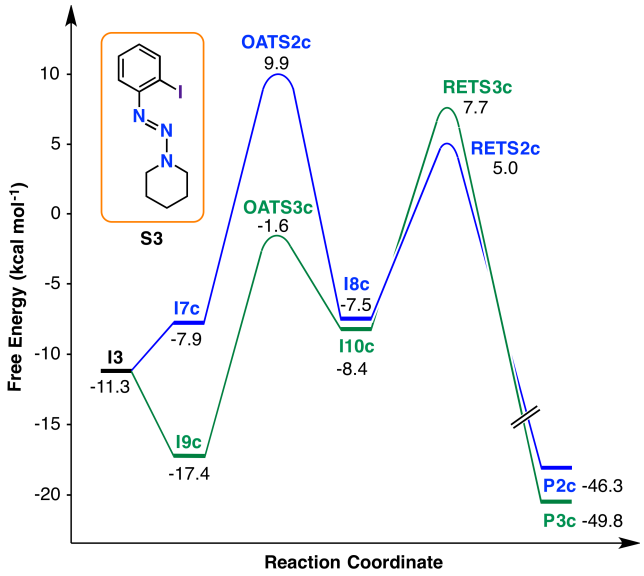

Scheme 6. Gibbs energy profiles (in kcal mol^{-1}) for Pathways 2 (blue) and 3 (green) in the copper-catalyzed cross-coupling of 1-((2-iodophenyl)diazenyl)piperidine (**S3**) with bromozinc-difluorophosphonate, starting from **I3**.

The coordination of substrate **S3** onto the copper atom of **I3** would produce the formation of intermediate **I7c**; this latter complex is slightly higher in energy than the separated reactants, indicating that the interaction between copper and the triazene directing group is not very strong although the Cu–N distance is quite short (2.22 Å). This could be due the steric hindrance introduced by the dangling piperidine ring, which is placed quite close to the phenanthroline ligand. The reaction should proceed by the C–I oxidative addition onto the copper atom. This stage is mediated by the corresponding **OATS2c** transition state, which requires further 17.8 kcal mol^{-1}. In this latter species the C_{ipso}–I, Cu–C_{ipso} and Cu–I distances of are 2.29, 2.19 and 2.82 Å, respectively, very similar to those shown by the benzoate substrates. Again, in **OATS2c** the distance between the copper atom and the directing group of the substrate becomes quite long (3.17 Å). After the oxidative addition the copper(III) complex **I8c** should be formed; this intermediate is found at a very similar energy to that of the previous intermediate **I7c** and has a square pyramid arrangement around the metal center, with one nitrogen atom of the phenanthroline ligand taking the axial position. The reaction may then continue by the C–C reductive elimination of the product; this transformation is governed by the corresponding transition state **RETS2c** that requires only 9.3 kcal mol^{-1}. Pathway 3 starts by the substrate

coordination onto the zinc fragment and the formation of intermediate **I9c**. As stated above, this process seems to be much favored over the formation of **I7c** since both intermediates show an energy difference of almost 10 kcal mol^{-1} in favor of **I9c**. In this latter complex the Zn–N distance is quite longer (2.34 Å) than those observed for the benzoate substrates, in which this distance remains around 2.15 Å. The reaction may then proceed by the oxidative addition of the Cu–I bond onto copper. This stage is controlled by the corresponding transition state **OATS3c** and requires a relatively low energy investment of 15.8 kcal mol^{-1}. The structural features of this transition state are very similar to those shown above for the analogous structures in Pathway 3 *i.e.* Cu–C_{ipso}, C_{ipso}–I and Cu–I distances of are 2.19, 2.32 and 2.74 Å, respectively. Once the oxidative addition barrier has been overcome intermediate **I10c** should be obtained. This complex displays a similar coordination pattern as that adopted by **I10**, with the CF_2 and the phenyl groups placed *cis* to each other in the equatorial plane and one of the phenanthroline nitrogens in the axial position. Species **I10c** is again less stable than the preceding intermediate (9 kcal mol^{-1}) but remains at an acceptable level. The reductive elimination process closes this catalytic cycle and delivers the final cyclometalated product **P3c** along with the initial catalyst. This process requires 16.1 kcal mol^{-1} and the associated transition state **RETS3c** is similar to that found for methyl 2-iodobenzate. The apparent Gibbs energy barriers for Pathways 2 and 3, computed as the energy difference between the resting state **I9c** and **OATS2c** or **RETS3c**, are 27.3 and 25.1 kcal mol^{-1}, respectively. This states that Pathway 3 should be the most likely to produce the final difluorinated product. As expected from the experimental data, and in spite of the small differences between the experimental and the calculated catalytic systems, the computed reaction barriers of methyl 2-iodobenzoate (**S**) and 1-((2-iodophenyl)diazenyl)piperidine (**S3**) are very similar: 24.9 and 25.1 kcal mol^{-1}, respectively, confirming the observed reactivity of the latter substrate in the cross-coupling reaction.

The reaction mechanism for the potential substrate phenyl 2-(2-iodophenyl)pyridine (**S4**) has been also computed (Scheme 7). The addition of substrate **S4** to intermediate **I3** is exergonic upon coordination to either metal center. However the energy difference between complexes **I7d** and **I9d** is quite large (9.4 kcal mol^{-1} in favor of the latter), indicating that the reaction should proceed, as observed before, by the binding of the substrate to the zinc atom *i.e.* following Pathway 3. Even so, Pathway 2 has been fully computed in order to complete the mechanistic picture. The C–I oxidative addition after the coordination of 2-(2-iodophenyl)pyridine onto the copper atom (**OATS2d**) requires 18.6 kcal mol^{-1}, a slightly lower value than that obtained for methyl 2-iodobenzoate (19.8 kcal mol^{-1}). The copper(III) intermediate formed after the oxidative addition (**I8d**) is less stable than the analogous structure obtained with methyl 2-iodobenzoate (**I8**) although both complexes have the same ligand arrangement, with the pyridyl group (or the carboxylate in **I8**) and one of the nitrogen atoms of phenanthroline placed *trans* to each other in the axial positions. This is probably because of the larger steric congestion introduced by the pyridyl group, which clashes with one of the rings of phenanthroline and forces the former to slightly tilt away from the copper atom. The reductive elimination barrier from **I8d** is quite

low and requires a small energy investment of 9.3 kcal mol^{-1}. The relevant distances in the oxidative addition (**OATS2d**) and reductive elimination (**RETS2d**) transition states along this pathway are quite similar to those obtained with methyl 2-iodobenzoate and therefore they will not be shown.

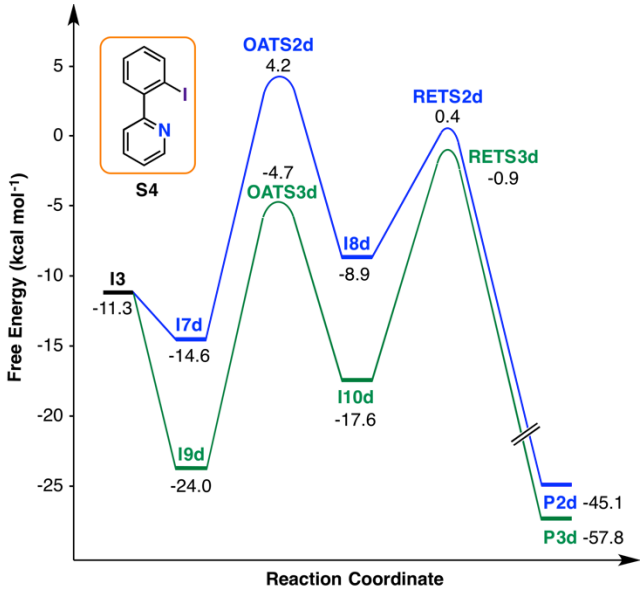

Scheme 7. Gibbs energy profiles (in kcal mol^{-1}) for Pathways 2 (blue) and 3 (green) in the copper-catalyzed cross-coupling of phenyl 2-(2-iodophenyl)pyridine (**S4**) with bromozinc-difluorophosphonate, starting from **I3**.

As mentioned above, in the first stage of Pathway 3, the 2-(2-iodophenyl)pyridine substrate coordinates to the zinc through the pyridyl nitrogen. This reaction step should produce intermediate **I9d**, which constitutes the lowest energy point along the reaction coordinate of the whole cross-coupling process. In this complex the Zn–N_{py} distance is again very short (2.15 Å), indicating a quite strong interaction between the catalytic species and the substrate. The reaction may proceed by the oxidative addition of the C–I bond onto the copper center; this process is mediated by the corresponding transition state (**OATS3d**) and requires 19.3 kcal mol^{-1}. After that the copper(III) intermediate **I10d** should be formed; this complex is similar to those shown before and displays a square pyramidal structure around the metal; again, one of the phenanthroline nitrogen donor atoms occupies the axial position while the difluorophosphonate and 2-phenylpyridine groups are placed *cis* to each other. The final reaction stage is the reductive elimination of the C–C bond to produce the corresponding cyclometalated product (**P3d**). This process is controlled by the reductive elimination transition state (**RETS3d**) that is located 16.7 kcal mol^{-1} above intermediate **I10d**; this magnitude is slightly lower to that obtained for the original methyl 2-iodobenzoate substrate (18.3 kcal mol^{-1}). As before, the relevant features of the oxidative addition and reductive elimination transition states along this pathway (**OATS3d** and **RETS3d**, respectively) are similar to those shown previously in Figure 2. The apparent reaction barrier for the cross-coupling reaction of 2-(2-iodophenyl)pyridine with the bromozinc-difluorophosphonate is 23.1 kcal mol^{-1},

computed as the Gibbs energy difference between **I9d** and **RETS3d**, and corresponds to that of Pathway 3. The overall barrier for Pathway 2, computed form the resting state (**I9d**) to the highest energy transition state (**OATS2d**), is 24.4 kcal mol^{-1}, indicating that this pathway is probably much less effective. Since the barrier for 2-(2-iodophenyl)pyridine (**S4**) is lower than that obtained for methyl 2-iodobenzoate (**S**) and 1-((2-Iodophenyl)diazenyl)piperidine (**S3**): 23.1, 24.9 and 23.7 kcal mol^{-1} respectively, a faster cross-coupling reaction should be expected when using the former as substrate.

CONCLUSION

The reaction mechanism of the copper-catalyzed cross-coupling of iodobenzoates with bromozinc-difluorophosphonate has been explored with DFT calculations. Three different pathways, arising from the original proposal of Zhang, have been studied. One of them is shown to be not operative because the zinc byproduct [ZnBrI(1,4-dioxane)$_2$] cannot be expelled into the reaction mixture. Keeping that fragment bound to the catalytic species throughout the reaction cycle seems to fix the problem. Even so the calculations indicate that the carboxylate directing group of methyl 2-iodobenzoate interacts preferentially with the zinc atom rather than with copper. This produces a new catalytic cycle that has a relatively low reaction barrier and still leads to the same final difluorinated product.

The computed catalytic cycle is also able to explain the experimentally observed reactivity of methyl 4-iodobenzoate, which produces a slow, although operative, reaction. In principle, the position of the directing group in this substrate should prevent the C–I activation to occur onto copper and thus the cross-coupling reaction with bromozinc-difluorophosphonate should not work. However, a similar pathway to that for methyl 2-iodobenzoate turns up if the benzoate interacts with the zinc fragment. This pathway allows the reaction to proceed and has a relatively large Gibbs energy barrier, which agrees with methyl 4-iodobenzoate producing a slow cross-coupling reaction.

Finally, the proposed mechanism has been successfully applied to predict whether other substrates could be able to engage in an analogous cross-coupling reaction with bromozinc-difluorophosphonate. The 1-((2-Iodophenyl)diazenyl)piperidine substrate, already employed in a very similar cross-coupling process, is likely to follow the same reaction pathway than methyl 2-iodobenzoate. These two substrates are computed to display very similar Gibbs energy barriers, in agreement with the experimental data. On the other hand, the potential 2-(2-iodophenyl)pyridine substrate, and most probably its derivatives, provides a way to prepare new difluorinated products. The computed overall Gibbs energy barrier for these nitrogen-directing substrates is smaller than that obtained for methyl 2-iodobenzoate indicating that faster, or lower temperature, cross-coupling reactions should be expected.

ASSOCIATED CONTENT

Supporting Information

Contains the detailed procedure to obtain the Gibbs energy values and the computed energy terms for all the species in the catalytic cycles. The supplemental file geometries.xyz contains the computed Cartesian coordinates of all of the molecules reported in this study. The file may be opened as a text file to read the coordinates, or opened directly by a molecular modeling program such as Mercury (version 3.3 or later, http://www.ccdc.cam.ac.uk/pages/Home.aspx) for visualization and analysis. This material is available free of charge via the Internet at http://pubs.acs.org.

AUTHOR INFORMATION

Corresponding Author

* E-mail: jesus.jover@qi.ub.es

ORCID

Jesús Jover: 0000-0003-3383-4573

Notes

The author declares no competing financial interest.

ACKNOWLEDGMENTS

This research has been supported by the Spanish Ministerio de Economía y Competitividad (MINECO, grant CTQ2015-68770-R).

REFERENCES

(1) (a) Clark, J. H.; Wails, D.; Bastock, T. W., *Aromatic Fluorination*. CRC Press: Boca Raton, FL, 1996; (b) Kirsch, P., *Modern Fluoroorganic Chemistry*. Wiley-VCH: Weinheim, 2004; (c) Uneyama, K., *Organofluorine Chemistry*. Blackwell: Oxford, UK, 2006; (d) Purser, S.; Moore, P. R.; Swallow, S.; Gouverneur, V. *Chem. Soc. Rev.* **2008**, 37, 320-330; (e) Ojima, I., *Fluorine in Medicinal Chemistry and Chemical Biology*. Wiley-Blackwell: Chichester, UK, 2009; (f) Wang, J.; Sánchez-Roselló, M.; Aceña, J. L.; del Pozo, C.; Sorochinsky, A. E.; Fustero, S.; Soloshonok, V. A.; Liu, H. *Chem. Rev.* **2014**, 114, 2432-2506.

(2) (a) Chen, P.; Liu, G. *Synthesis* **2013**, 45, 2919-2939; (b) Wu, X.-F.; Neumann, H.; Beller, M. *Chem. Asian J.* **2012**, 7, 1744-1754; (c) Liu, H.; Gu, Z.; Jiang, X. *Adv. Synth. Catal.* **2013**, 355, 617-626; (d) Egami, H.; Sodeoka, M. *Angew. Chem. Int. Ed.* **2014**, 53, 8294-8308; (e) Merino, E.; Nevado, C. *Chem. Soc. Rev.* **2014**, 43, 6598-6608; (f) Gouverneur, V.; Seppelt, K. *Chem. Rev.* **2015**, 115, 563-565.

(3) (a) Besset, T.; Poisson, T.; Pannecoucke, X. *Chem. - Eur. J.* **2014**, 20, 16830-16845; (b) Feng, Z.; Min, Q.-Q.; Xiao, Y.-L.; Zhang, B.; Zhang, X. *Angew. Chem. Int. Ed.* **2014**, 53, 1669-1673; (c) Feng, Z.; Xiao, Y.-L.; Zhang, X. *Org. Chem. Front.* **2014**, 1, 113-116; (d) Min, Q.-Q.; Yin, Z.; Feng, Z.; Guo, W.-H.; Zhang, X. *J. Am. Chem. Soc.* **2014**, 136, 1230-1233; (e) Xiao, Y.-L.; Guo, W.-H.; He, G.-Z.; Pan, Q.; Zhang, X. *Angew. Chem. Int. Ed.* **2014**, 53, 9909-9913; (f) Belhomme, M.-C.; Besset, T.; Poisson, T.; Pannecoucke, X. *Chem. - Eur. J.* **2015**, 21, 12836-12865; (g) Ivanova,

M. V.; Bayle, A.; Besset, T.; Poisson, T.; Pannecoucke, X. *Angew. Chem. Int. Ed.* **2015**, 54, 13406-13410; (h) Xu, P.; Guo, S.; Wang, L.; Tang, P. *Synlett* **2015**, 26, 36-39; (i) Pannecoucke, X.; Poisson, T. *Synlett* **2016**, 27, 2314-2326.
(4) (a) Blackburn, G. M.; Kent, D. E.; Kolkmann, F. *J. Chem. Soc. Chem. Commun.* **1981**, 1188-1190; (b) Blackburn, G. M.; Kent, D. E.; Kolkmann, F. *J. Chem. Soc. Perkin Trans.* **1984**, 1119-1125; (c) Howson, W.; Hills, J. M.; Michael Blackburn, G.; Broekman, M. *Bioorg. Med. Chem. Lett.* **1991**, 1, 501-502; (d) Ong, J. X.; Yap, C. W.; Ang, W. H. *Inorg. Chem.* **2012**, 51, 12483-12492.
(5) Feng, Z.; Chen, F.; Zhang, X. *Org. Lett.* **2012**, 14, 1938-1941.
(6) Yokomatsu, T.; Murano, T.; Suemune, K.; Shibuya, S. *Tetrahedron* **1997**, 53, 815-822.
(7) Frisch, M. J.; Trucks, G. W.; Schlegel, H. B.; Scuseria, G. E.; Robb, M. A.; Cheeseman, J. R.; Scalmani, G.; Barone, V.; Mennucci, B.; Petersson, G. A.; Nakatsuji, H.; Caricato, M.; Li, X.; Hratchian, H. P.; Izmaylov, A. F.; Bloino, J.; Zheng, G.; Sonnenberg, J. L.; Hada, M.; Ehara, M.; Toyota, K.; Fukuda, R.; Hasegawa, J.; Ishida, M.; Nakajima, T.; Honda, Y.; Kitao, O.; Nakai, H.; Vreven, T.; Montgomery, J., J. A.; Peralta, J. E.; Ogliaro, F.; Bearpark, M.; Heyd, J. J.; Brothers, E.; Kudin, K. N.; Staroverov, V. N.; Kobayashi, R.; Normand, J.; Raghavachari, K.; Rendell, A.; Burant, J. C.; Iyengar, S. S.; Tomasi, J.; Cossi, M.; Rega, N.; Millam, N. J.; Klene, M.; Knox, J. E.; Cross, J. B.; Bakken, V.; Adamo, C.; Jaramillo, J.; Gomperts, R.; Stratmann, R. E.; Yazyev, O.; Austin, A. J.; Cammi, R.; Pomelli, C.; Ochterski, J. W.; Martin, R. L.; Morokuma, K.; Zakrzewski, V. G.; Voth, G. A.; Salvador, P.; Dannenberg, J. J.; Dapprich, S.; Daniels, A. D.; Farkas, Ö.; Foresman, J. B.; Ortiz, J. V.; Cioslowski, J.; Fox, D. J. *Gaussian09, Revision D.01*, Gaussian, Inc.: Wallingford CT, **2009**.
(8) (a) Lee, C.; Yang, W.; Parr, R. G. *Phys. Rev. B* **1988**, 37, 785-789; (b) Miehlich, B.; Savin, A.; Stoll, H.; Preuss, H. *Chem. Phys. Lett.* **1989**, 157, 200-206; (c) Becke, A. D. *J. Chem. Phys.* **1993**, 98, 5648-5652.
(9) (a) Ditchfield, R.; Hehre, W. J.; Pople, J. A. *J. Chem. Phys.* **1971**, 54, 724-728; (b) Hehre, W. J.; Ditchfield, R.; Pople, J. A. *J. Chem. Phys.* **1972**, 56, 2257-2261; (c) Hariharan, P. C.; Pople, J. A. *Theor. Chem. Acc.* **1973**, 28, 213-222.
(10) (a) Dunning, T. H.; Hay, P. J., In *Modern Theoretical Chemistry*, Schaefer III, H. F., Ed. Plenum: New York, 1976; Vol. 3, pp 1-28; (b) Bergner, A.; Dolg, M.; Küchle, W.; Stoll, H.; Preuss, H. *Mol. Phys.* **1993**, 80, 1431-1441.
(11) (a) Tannor, D. J.; Marten, B.; Murphy, R.; Friesner, R. A.; Sitkoff, D.; Nicholls, A.; Honig, B.; Ringnalda, M.; Goddard, W. A. *J. Am. Chem. Soc.* **1994**, 116, 11875-11882; (b) Marten, B.; Kim, K.; Cortis, C.; Friesner, R. A.; Murphy, R. B.; Ringnalda, M. N.; Sitkoff, D.; Honig, B. *J. Phys. Chem.* **1996**, 100, 11775-11788.
(12) Marenich, A. V.; Cramer, C. J.; Truhlar, D. G. *J. Phys. Chem. B* **2009**, 113, 6378-6396.
(13) Grimme, S.; Antony, J.; Ehrlich, S.; Krieg, H. *J. Chem. Phys.* **2010**, 132, 154104.
(14) (a) Peterson, K. A.; Figgen, D.; Goll, E.; Stoll, H.; Dolg, M. *J. Chem. Phys.* **2003**, 119, 11113-11123; (b) Peterson, K. A.; Puzzarini, C. *Theor. Chem. Acc.* **2005**, 114, 283-296; (c) Balabanov, N. B.; Peterson, K. A. *J. Chem. Phys.* **2005**, 123, 064107.
(15) (a) Jover, J. *ACS Catal.* **2014**, 4, 4389-4397; (b) Jover, J.; Maseras, F. *J. Org.Chem.* **2014**, 79, 11981-11987; (c) Jover, J.; Spuhler, P.; Zhao, L.; McArdle, C.; Maseras, F. *Cat. Sci. Technol.* **2014**, 4, 4200-4209; (d) Jover, J. *J. Chem.* **2015**, 2015, 8; (e) Jover, J. *Phys. Chem. Chem. Phys.* **2017**, 19, 29344-29353.

(16) (a) Perdew, J. P.; Burke, K.; Ernzerhof, M. *Phys. Rev. Lett.* **1996**, 77, 3865-3868; (b) Perdew, J. P.; Burke, K.; Ernzerhof, M. *Phys. Rev. Lett.* **1997**, 78, 1396; (c) Adamo, C.; Barone, V. *J. Chem. Phys* **1999**, 110, 6158-6169.
(17) (a) Becke, A. D. *J. Chem. Phys.* **1997**, 107, 8554-8560; (b) Grimme, S. *J. Comp. Chem.* **2006**, 27, 1787-1799.
(18) (a) Bertz, S. H.; Cope, S.; Dorton, D.; Murphy, M.; Ogle, C. A. *Angew. Chem. Int. Ed.* **2007**, 46, 7082-7085; (b) Yoshikai, N.; Nakamura, E. *Chem. Rev.* **2012**, 112, 2339-2372; (c) Casitas, A.; Ribas, X. *Chem. Sci.* **2013**, 4, 2301-2318.
(19) (a) Ichiishi, N.; Canty, A. J.; Yates, B. F.; Sanford, M. S. *Organometallics* **2014**, 33, 5525-5534; (b) Romine, A. M.; Nebra, N.; Konovalov, A. I.; Martin, E.; Benet-Buchholz, J.; Grushin, V. V. *Angew. Chem. Int. Ed.* **2015**, 54, 2745-2749; (c) Zhang, S.-L.; Bie, W.-F. *RSC Advances* **2016**, 6, 70902-70906; (d) Rovira, M.; Jasikova, L.; Andris, E.; Acuna-Pares, F.; Soler, M.; Guell, I.; Wang, M.-Z.; Gomez, L.; Luis, J. M.; Roithova, J.; Ribas, X. *Chem. Commun.* **2017**, 53, 8786-8789.
(20) Kozuch, S.; Shaik, S. *Acc. Chem. Res.* **2011**, 44, 101-110.

TABLE OF CONTENTS GRAPHIC